Journal of Materials Chemistry A

Accepted Manuscript

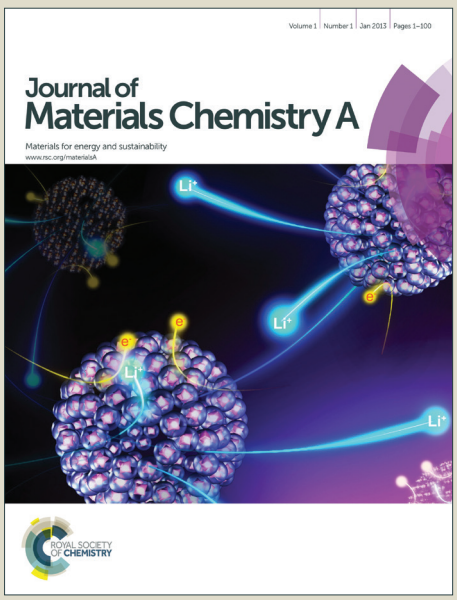

ROYAL SOCIETY OF CHEMISTRY

www.rsc.org/materialsA

Journal Name

RSCPublishing

ARTICLE

Li- and Na-reduction products of *meso*-Co_3O_4 form high-rate, stably cycling battery anode materials

Cite this: DOI: 10.1039/xoxxoooooox

Received ooth January 2012,
Accepted ooth January 2012

DOI: 10.1039/xoxxoooooox

www.rsc.org/

Kyle. C. Klavetter[a], Stephany Garcia[b], Naween Dahal[b], Jonathan L. Snider[a], J. Pedro de Souza[a], Trevor H. Cell[c], Mark A. Cassara[a], Simon M. Humphrey[b], Adam Heller[a], C. Buddie Mullins[a,c,d,*]

High surface area (367 m^2 g^{-1}) *meso*-porous Co_3O_4 was investigated as the precursor of the anode material for lithium and also sodium ion batteries. Co_3O_4 is considered a potential anode material due to its theoretical capacity of 890 mAh g^{-1}, over twice that of graphite. This comparatively higher capacity can be safely charged at rapid rates owing to a relatively high Li-insertion potentials, but, consequently, the discharged energy is yielded at an average potential near 2 V *vs* Li/Li^+, with full Li-extraction achieved over a continuum of potentials up to 3 V. The products of the lithium reduction of Co_3O_4 cycle stably from 0.01 – 3.0 V *vs* Li/Li^+ with 600-900 mAh/g capacity retention at *C* rates from 1-5; the products of its sodium reduction cycle stably from 0.01 – 3.0 V *vs* Na/Na^+ at C-rates up to 1*C* with a lower 150-400 mAh/g capacity retention owing to greater ionic impedance. TEM, SAED and XRD were used to examine the cycled material and the stable performance is attributed to finding that the mesoporous structure is retained. Evaluation of five electrolyte formulations testing EC, FEC and Cl-EC co-solvents showed that the stable *meso*-porous structure was best cycled with 5% FEC in EC:DEC at high charge/discharge rates, retaining 77% of its initial capacity at 5*C* in a rate test.Comparison of the AC impedance spectra and of the XPS of the SEIs formed in the presence and in the absence of 5 vol. % FEC shows that the SEI formed in the presence of FEC contains fluoride and its carbonate layer is thinner than that formed in its absence, resulting in lesser impedance to Li and Na migration through the SEI and facile ion de-solvation, improving the cycling performance. In cycling stability tests with EC:DEC, irregular cycling behaviour attributable to abrupt rises in cell resistance was regularly observed after testing over a few hundred cycles. Long-term cycling irregularities are inhibited by halogenated solvents and completely eliminated by adding fluoroethylene carbonate (FEC).

Affiliations

[a] McKetta Department of Chemical Engineering, 200 E. Dean Keeton St. Stop C0400 Austin, TX 78712, USA

[b] Department of Chemistry and Biochemistry, The University of Texas at Austin, 1 University Station A5300, Austin, USA

[c] Department of Chemistry, 105 E. 24th St. Stop A5300 Austin, TX 78712, USA

[d] Texas Materials Institute and Center for Electrochemistry, The University of Texas at Austin, Austin, TX 78712, USA

[*] mullins@che.utexas.edu

Introduction

To charge to higher capacities at faster rates in lithium ion batteries, energy storage by a means other than intercalation into graphite is required. Graphite, the commonly used anode active material with a low practical capacity of near 360 mAh g^{-1}, charges at low potentials vs Li/Li^+ and so requires a relatively slow constant current, constant voltage charge method in order to avoid the hazard of electroplating of lithium and dendrite formation.

Potential rapidly charged anode materials being considered for rechargeable batteries include Li-reduced transition metal oxides that result in the formation of mixtures of transition metal, transition metal oxide and Li_2O. These anode materials charge to higher capacities at higher potentials *vs* the Li/Li^+ redox couple, resulting in a more safe charge at faster rates but

with necessarily lower energy as a consequence of full discharge usually being achieved only by extending the discharge up to 3.0 V. Examples of such transition metal oxide anode materials include nanoparticles of Ni formed by Li-reduction of NiO[1], of Fe and FeO formed by Li-reduction of Fe_2O_3[2] and of Co and CoO by Li-reduction formed of Co_3O_4. Because of its theoretical capacity of 890 mAh g^{-1} (although with a relatively high discharge potential of near 2 V vs Li/Li^+), cobalt oxide has been pursued as an anode material and tested in a variety of morphologies – nanowire[3,4], nanorod[5,6], nanocage[7,8,9], leaf-like[10], *meso*-porous[11,12,13], platelet[14], hollow sphere[15], carbon-composite[16,17,18], micro/nano composite[19] – and high capacity retention at high rates has been obtained [10,12,13,15,16]. For this material in any of these forms tested, the onset of capacity fade at higher rates or during the course of cycling is commonly attributed to particle agglomeration leading to cobalt segregation into electrically isolated nanoscale domains, electrode crack formation and delamination from the current collector and/or SEI growth leading to increasing overpotentials.

From consideration of Co_3O_4 in nanowire and *meso*-porous morphologies, Bruce and coworkers[20] suggested that higher and more stable capacities for a cobalt oxide-based anode could be realized if a *meso*-porous particle could be found which retained its structure upon Li-reduction, avoiding Co aggregation and providing for reversible, fast Li-ion transport through the pores. In their study, the originally *meso*-porous Co_3O_4 was reduced to *meso*-porous CoO in the first cycle, but after 50 cycles the *meso*-porous structure was lost and significant capacity fade was observed. Recently, Xiao *et al.*[13] studied a low surface area (27 m^2 g^{-1}) *meso*-porous Co_3O_4 reporting good rate capability and a very high 1600 mAh g^{-1} capacity which was retained after 100 cycles (at 100 mA g^{-1}). Also recently, Li *et al.*[11] reported full capacity retention (600 mAh g^{-1}) through 500 cycles at a rate of 500 mA g^{-1} with a *meso*-porous Co_3O_4 based anode, although their composite electrode required nearly an equal mass of graphene, a high content of a material with a cost 3-4 orders of magnitude higher than the commercially used carbon black conductive additive.

Here we report stable, high rate capacity cycling results of high surface area (367 m^2 g^{-1}) *meso*-porous Co_3O_4 for Li and for Na ion half cells. The cycling performance is primarily attributed to the individual particles retaining their *meso*-porous structure upon repeated charging/discharging, as established by high-resolution transmission electron micrography (TEM). With powder X-ray diffraction and selected area electron diffraction (SAED), we show that the cycled *meso*-porous particle lacks long range order but reverts upon discharge at highly oxidizing potentials to an inhomogeneous mixture of CoO and Co_3O_4.

Upon discovering the stable morphology of the active material particle in the electrodes, we attempted to improve the performance of the electrode by testing of alternative electrolyte formulations, as has been done for other lithium-ion battery anode materials.[21,22,23] Here, fluoroethylene carbonate (FEC) and chloroethylene carbonate (Cl-EC) as electrolyte co-solvents or additives allowed for higher capacity retention at high charge/discharge rates, increased coulombic efficiencies (CE), further improved cycling stability and decreased risk of internal shorting from dendrite formation. FEC was added because numerous reports have shown that it improves the calendar life and cycling performance of both Li- and Na-ion anodes, while Cl-EC was added because of its reported beneficial effect on improving coulombic efficiency[24], a metric for which some otherwise high-performing cobalt oxide-based anodes have performed poorly[10,15]. Employing FEC or Cl-EC, we survey alternative formulations to the conventional ethylene carbonate (EC) based electrolyte for cobalt oxide based electrodes. The advantages of the halogen-containing electrolytes over the conventional EC-based electrolyte include: (1) inhibited or eliminated cycling irregularities typical of long-term behaviour of electrodes tested with EC:DEC and (2) the lesser resistance to ion transport of the solid electrolyte interphases (SEIs) they form, as seen in the AC impedance spectra and X-ray photoelectron spectra (XPS) characterization of the SEIs.

Experimental

Materials

Synthesis of the *meso*-porous Co_3O_4 and the quality control evaluation done to verify its morphology, surface area and phase was performed as described elsewhere by Dahal *et al.*[25]

Electrochemical testing

An aqueous slurry of *meso*-porous Co_3O_4 (60 wt %), 90 kDa carboxymethyl cellulose (Sigma, 20 wt %) binder, and Super P Li conductive carbon (Timcal, 20 wt %) was slurry cast onto copper foil (MTI, 10 μm) and dried in a vacuum oven at 120 °C for at least 6 h. This film formed the working electrodes of CR 2032 coin-type cells and each electrode had a Co_3O_4 mass loading of 0.6-0.8 mg cm^{-2}. Scanning electron micrographs (SEM) of a typical electrode (uncycled), showing cross-section and distribution of active material and Super-P Li conductive additive are shown in Fig. S1a-b, ESI†.

The half cells were assembled in an argon-filled glovebox (O_2 less than 0.1 ppm, H_2O < 3.6 ppm) with Li foil (Alfa) or Na foil (Sigma) as the counter and reference electrode and Celgard 2400 polypropylene membrane as the separator. Additional testing performed on electrodes of composition 80:10:10 weight ratio had mass loadings of 0.9-1.0 mg cm^{-2} of active material. The electrolyte materials, ethylene carbonate (EC, Sigma), anhydrous diethyl carbonate (DEC, Sigma), chloroethylene carbonate (Cl-EC, TCI), fluoroethylene carbonate (FEC, Solvay Fluor) and $LiPF_6$ (BASF) were used as received. Electrolytes were preserved against moisture contamination by the addition of molecular sieves to the storage vials.

Electrochemical measurements were performed on an Arbin BT 2043 or BT 2143 multichannel battery testing system. Charge (ion-insertion into the anode) and discharge (ion-

extraction) were performed between 0.01 and 3 V *vs* the Li/Li^+ or Na/Na^+ redox couple with the theoretical capacity defined as 890 mAh g^{-1} (1*C* = 0.89 A/g). For each cell, a conditioning cycle at *C*/20 was done prior to testing.

AC impedance spectra were obtained from cells cycled at a conditioning *C*/20 rate followed by 10 cycles at a *C*/10 rate. On the tenth cycle at a *C*/10 rate, the cell was evaluated at two conditions: 1) after being charged at constant current (*C*/10) and held at constant voltage (100 mV, a voltage selected in order to avoid electroplating lithium) until the current dropped to below C/20 and 2) after being discharged to 3 V and then allowed to come to thermodynamic equilibrium after resting for greater than 12 h. The spectra were analysed in ZView (*Scribner Associates*)[26] and a best fit was made for the entire range of collected data (100k to 0.01 Hz, 5 mV perturbations).

Microscopy

Low-resolution transmission electron microscopy (LR-TEM) was performed for each of the electrode/electrolyte combinations using a FEI Tecnai Spirit BioTwin TEM operated at 80 kV to evaluate the condition of the *meso*-porous particle in its native electrode environment after preparation using an ultramicrotome sectioning procedure (as described elsewhere).[27] Select, additional imaging of these sectioned electrodes was done on a field emission JEOL 2010F TEM operated at 200 kV for higher resolution micrographs. Selected area electron diffraction (SAED) patterns were obtained from particles drop cast onto lacey carbon grids (*SPI*).

X-ray photoelectron spectroscopy (XPS)

XPS measurements were conducted on electrodes that had been cycled to a fully discharged state, after ten cycles at a *C*/10 rate initiated by a *C*/20 conditioning cycle. This number of cycles was selected to allow for analysis of a fully formed SEI (the SEI primarily develops during the first 2-3 cycles as indicated by the CE) but to avoid micron-scale dendritic growths which were observed to develop after many cycles. The cells were opened in the glovebox using plastic pliers (I-V Products) and the electrodes were placed into vials filled with DEC in order to wash off the residual $LiPF_6$ salt. The electrodes were transferred from the glovebox to the XPS analysis instrument (Kratos Axis Ultra) without exposure to air using a home-built delivery vessel (described elsewhere).[28]

The SEI surfaces were characterized utilizing a monochromatic Al *K*α X-ray source ($h\nu$ = 1486.5 eV) with and without the use of a charge neutralizer. The use of a charge neutralizer did not appreciably alter the shape and intensity of the spectra and the spectra collected without charge neutralization are therefore reported. The peak assignments of the XPS spectra collected for the Li-ion electrodes were calibrated to the C 1*s* sp^3 peak at 284.5 eV and checked by considering the resulting alignment of the F 1*s* LiF peak at 684.6 eV and P 2*p* P-O/P=O and P-F peaks at 134 eV and 136 eV, respectively.[29] The peak assignments for the Na-ion electrodes were similarly calibrated to the C 1*s* sp^3 peak at 284.5 eV and references for the Li-ion and Na-ion peak assignments are tabulated in S-Tables 1a-b, ESI†.

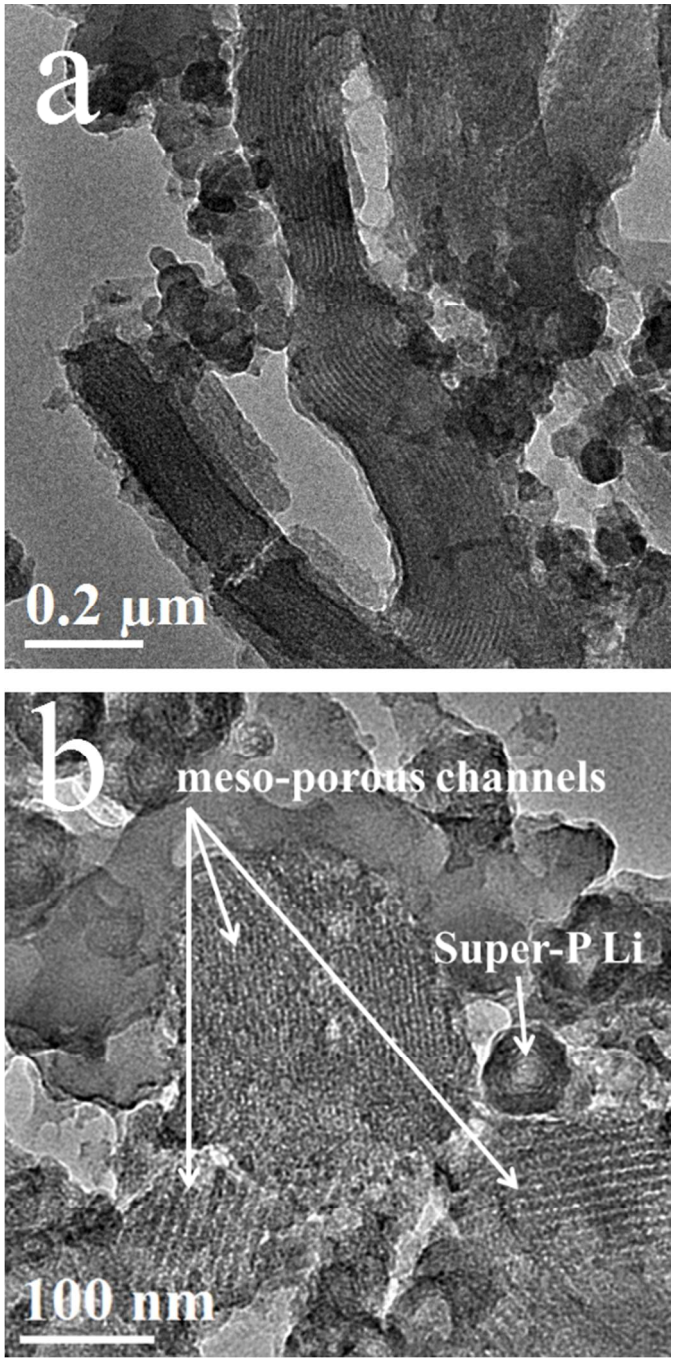

Fig. 1 TEM of ultramicrotomed cross-sections of electrodes in the discharged state after 250 cycles at 1*C* (a) showing the retention of the *meso*-porous channels in a few particles aligned parallel to the viewing plane and (b) indicating meso-porous particles and Super-P Li conductive additive particle.

Results and Discussion

The *meso*-porous particle

In this study we targeted a high surface area *meso*-porous mixed Co(II)-Co(III) oxide in an effort to improve the capacity retention of a cobalt oxide based lithium or sodium ion anode operated at high rates. As reported in the description of its synthesis,[25] this *meso*-porous structure exhibits a very high N_2 BET surface area of *ca.* 367 m^2 g^{-1}. The material was prepared *via* a soft template synthesis using sacrificial surfactant templates to obtain SBA-15-like Co_3O_4; the material features *meso*-channels aligned parallel to the long axis of the particle with regular, cylindrical-shaped pores with an average diameter measured to be 10.0 nm and wall thickness of 8.3 nm. This structure is suited to accommodate the volumetric change associated with charge and discharge as well as to enhance ion access to the active material by shortening diffusion lengths and by providing channels for more rapid liquid-phase ion transport into the bulk of the particle.

The *meso*-porous particles studied here are promising for use in Li- or Na-ion batteries because their structure is preserved through many charge/discharge cycles despite the effects of energy storage via a conversion reaction. By means of XRD[30,31] and XPS[31] characterization, the conversion reaction has been shown to proceed by initially charging the mixed Co(II)-Co(III) oxide to $Li_xCo_3O_4$, then to CoO + Li_2O and finally to Co + Li_2O,[30] before discharging to give CoO.[20] However, the electrochemical charge after the CoO phase is reached occurs through amorphous phases (or through crystalline phases with only short-range order), limiting the extent to which these phase transitions can be currently described or, importantly, compared for cobalt oxide materials with varying morphologies. Currently, there exists no XRD data describing the subsequent discharge phase transitions except at a state of full discharge. This is significant, for after many cycles, the conventional explanation for capacity fade is that the Co formed during charging becomes segregated into electrically isolated nanoclusters, as shown using TEM and SAED by Bruce's group in their study of *meso*-porous and nanowire-cluster cobalt oxide particles.[20] However, Kang *et al.*[31] found that through 100 cycles at a 1*C* rate, their Co_3O_4 based electrode cycled stably and that the particle discharged to a polycrystalline Co_3O_4 phase. By evaluating these contrasting reports, a possible indicator of the degree of cycling stability for a particular cobalt oxide morphology was considered be the condition of the morphology as well as the phase of the active material at full discharge.

In our study we initially obtained TEM images of the ultramicrotomed cross-section of cycled electrodes (Fig 1, electrode tested in 5% FEC in EC:DEC electrolyte formulation) which surprisingly showed that the original meso-porous channels remained intact despite prolonged cycling (250 cycles testing at a 1*C* rate, Fig. S2, ESI†). TEM of similarly cycled electrodes in the other electrolyte formulations are shown in Fig. S3a-d, ESI†, and for each electrode/electrolyte

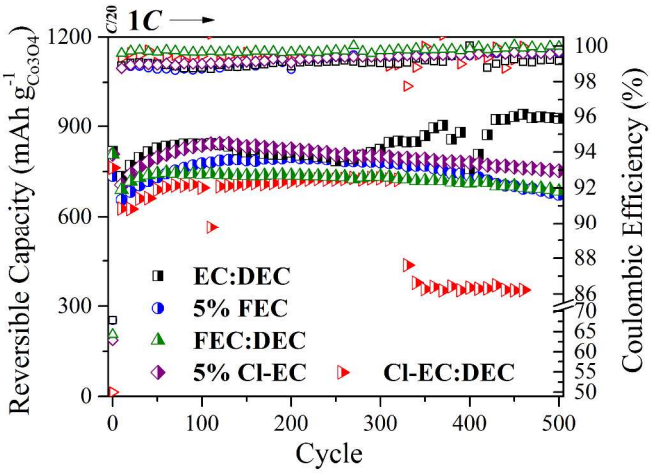

Fig. 2 Cycling test at 1*C* rate for 500 cycles following *C*/20 conditioning cycle in half cell of *meso*-porous Co_3O_4 based electrodes *vs* Li-foil with 1M $LiPF_6$ in EC:DEC, 5% FEC in EC:DEC, FEC:DEC, 5% Cl-EC in EC:DEC or Cl-EC:DEC electrolyte formulations.

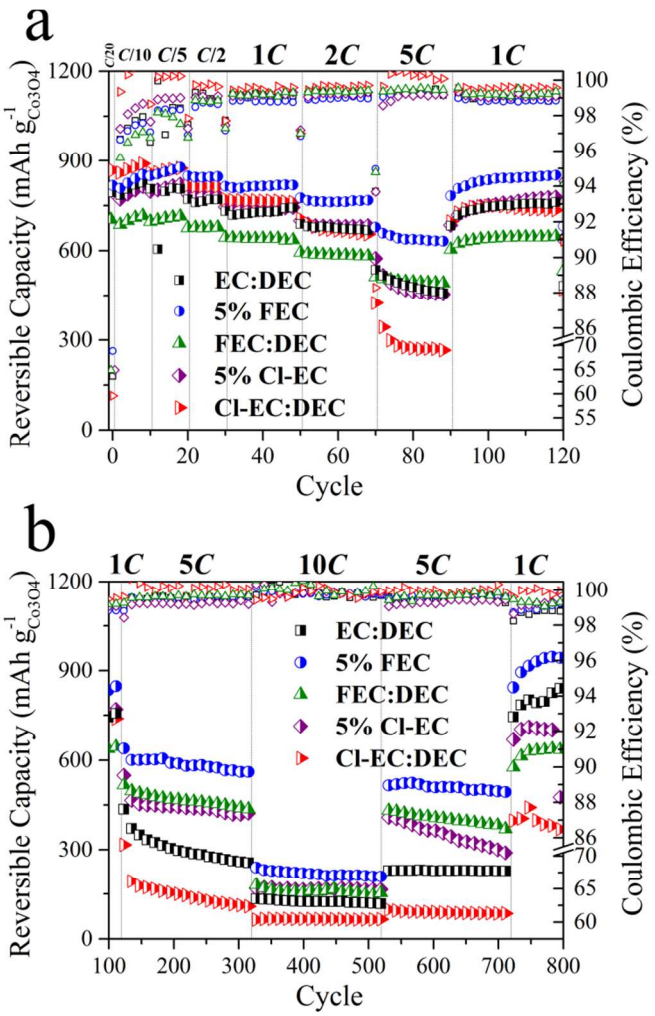

Fig. 3 Cycling test at *C*-rates from 0.1-10 through 800 cycles in half cell of *meso*-porous Co_3O_4 based electrodes *vs* Li-foil with 1M $LiPF_6$ in EC:DEC, 5% FEC in EC:DEC, FEC:DEC, 5% Cl-EC in EC:DEC or Cl-EC:DEC electrolyte formulations. Test results shown in (a) are continued in (b).

combination tested, we find that the particles studied here retain their original *meso*-porous, channeled morphology.

The preservation of the *meso*-porous morphology correlates with the reversible electrochemical cycling observed, and XRD was performed *ex-situ* to characterize the phase transitions responsible for stable cycling behavior. Surprisingly, at a full state of discharge after 10 cycles, no diffraction peaks were detected even with lengthy dwell times when performing characterization of the film upon the copper current collector or from a powder sample removed from the tested film (done so as to avoid interfering signal from the copper substrate). When long-range order was found absent in the discharged *meso*-porous material (XRD pattern shown in Fig. S4, ESI†), we endeavored to characterize the short-range structure by performing SAED. It was observed that upon discharge the *meso*-porous structure reverts to a generally amorphous material (Fig. S5a-b, ESI) containing some CoO and Co_3O_4 nanocrystals. In Fig. S5c-d, ESI, we find evidence for the existence of CoO which in this particular particle presents a nanocrystalline diffraction pattern with six-fold symmetry as observed due to its orientation along the <1 -1 1> zone axis.[32] However, after extensive searching, SAED showing the Co_3O_4 nanocrystalline phase was found to exist in other particles (Fig. S5e-f, ESI†).

Upon finding that the discharged condition of the *meso*-porous particle could not be identified as a homogenous phase, we attempted to characterize the full extent of the phase transitions undergone throughout the charge/discharge process and for this constructed an *in-situ* coin cell similar to that reported by Rhodes et al.[33] The cell design described by Rhodes et al. was modified here in order to minimize x-ray attenuation through the copper-coated polyethylene terephthalate (PET, commercially known as Mylar) window. By considering the relative intensity of signal derived from comparable electrode films made using the *meso*-porous particles and using commercial nanopowder (*Sigma*, less than 50 nm), we found that the uncycled *meso*-porous particles were weakly crystalline. Accordingly, the x-ray permeable window was here constructed using a thinner PET disk (50 μm *vs* 125 μm) and the thermally evaporated copper coating was reduced from 600 nm to 200 nm thickness.

In-situ characterization of the *meso*-porous electrode was performed during its first cycle of charging *via* linear voltammetry at 0.05 mV/s. However, the negligible signal obtained during this characterization precluded identification of the phase transitions for the *meso*-porous particle based electrode. In contrast, from the *in-situ* spectra recorded from characterization of the more strongly crystalline nanopowder based electrode (Fig. S6, ESI†), we observed a similar result to that of the findings of Larcher et al., showing that the cobalt oxide based electrode transitions through the CoO phase during initial charge and that subsequent electrochemical reactions proceed through amorphous phase transitions.

Li-ion cycling stability

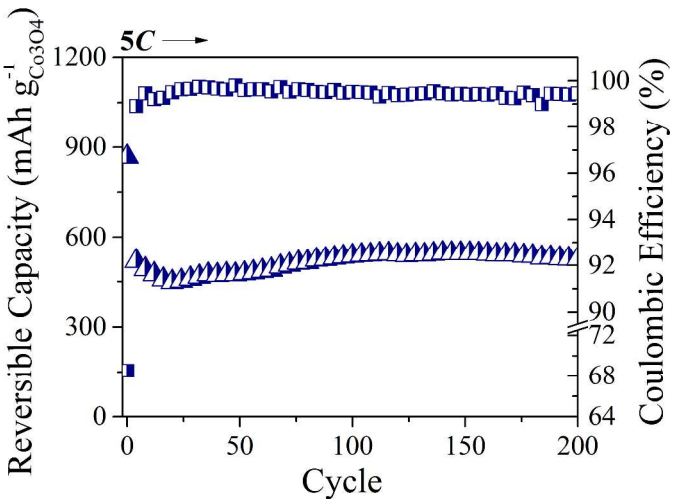

Fig. 4 Cycling test at 5*C* for 80% *meso*-porous Co_3O_4 (1.0 mg/cm^2 loading) / 10% Super-P Li / 10% CMC_{90kDa} electrode in 1M $LiPF_6$ in 5% FEC in EC:DEC electrolyte.

The result of the retention of bulk *meso*-porous morphology of the active material is relatively stable cycling behavior with each five of the electrolyte formulations tested (Fig. 2). To minimize the coulombic inefficiencies leading to SEI build-up and comparatively poor capacity retention at high rates – common consequences[27,34,35] of pairing a conventional EC-based electrolyte with a non-graphite based anode – cycling tests were designed to probe the effect of pairing the *meso*-porous Co_3O_4-based electrode with electrolytes formulated with FEC or Cl-EC as additives or as co-solvent substitutes for EC.

In this study, the cycling tests performed on *meso*-porous Co_3O_4-based electrodes were designed to indicate the most advantageous electrolyte by comparative assessment of the metrics of stability, initial coulombic efficiency and coulombic efficiency over long lifetime – 500 cycles at 1*C* (Fig. 2) – and capacity retention at variable *C*-rates (Fig. 3a,b).

Although not commonly reported, the value of a prolonged stability test like that presented in Fig. 2 is that long-term stability trends which might not be easily recognized from short-term tests may be identified. While at least three electrodes were tested for each cycling test, we found that after the first hundred cycles of testing there were only certain combinations of electrode/electrolyte for which consistent performance was observed. For example, the electrodes tested in the FEC:DEC or 5% FEC in EC:DEC electrolyte formulations performed consistently, but deviations were observed in the performance of the electrodes tested in the other formulations. In the case of those electrodes tested in EC:DEC, these deviations may be ascribed the electroplating of lithium which is believed to unpredictably significantly impact cell cycling at some point after about the first couple hundred cycles. More on this point is discussed below.

In the case of the electrodes tested using Cl-EC as an additive, the onset of capacity fade is also variable. When using Cl-EC as a co-solvent, we observed that the cycling deviations arise in unpredictable cell failure, in which the capacity

suddenly drops over the span of a several cycles, a symptom possibly due to a sudden rise in resistance to ion transport through what was found by AC impedance spectroscopy to be a high-impedance SEI. When only the first hundred cycles of testing were considered, these inconsistencies are obscured, preventing such analysis despite providing a more repeatable (albeit truncated) dataset.

We believe that data collected in a long-term cycling test, while containing deviations (some of which we do not understand) is important to report, particularly because the existence of inconsistencies in the testing of certain formulations of electrolyte is powerful evidence indicating their ineffectiveness. Further, as will be discussed for the electrodes tested in EC:DEC, these inconsistencies can sometimes be attributed to electroplating of lithium, a serious safety hazard and one which does not necessarily present except during prolonged testing.

To illustrate the difference in perspective which would result from consideration of a shortened, 100-cycle test *vs* the 500-cycle dataset reported here, we observe that in the 1*C* test runs shown in Fig. 2, the maximum 1*C* capacity is found at near the 100th cycle for each of the 5 electrode/electrolyte combinations tested except for that with the FEC:DEC electrolyte. Upon extended testing at 1*C* through 500 cycles, the effects of the alternative electrolyte formulations are clearly observed. Through 325 cycles, the most stable cycling electrode was tested with the Cl-EC:DEC electrolyte: before its capacity unexpectedly fell to *c*. 350 mAh g^{-1} through a transition of several cycles, the capacity retention at 325 cycles was 98% of its maximum 1*C* capacity (and 94% of the *C*/20 conditioning cycle capacity). When tested at lower mass loadings (near 0.4 mg cm^{-2}), this electrode was found to perform stably through 500 cycles (Fig. S7, ESI†), this attributable to the lower resistance through a thinner electrode. The FEC:DEC formulation best promoted stable cycling with capacity retention of 92% of its maximum 1*C* capacity (and 85% of the *C*/20 conditioning cycle capacity) with the highest average CE of 99.6%. These higher long-term efficiencies coincided with marginally lower initial, first cycle CE (for the conditioning cycle run at C/20) for which the EC:DEC and 5% FEC formulations led to the lowest irreversible losses (CE near 68%). The FEC:DEC and 5% Cl-EC formulations had first cycle CE's of about 65% and the highest irreversible losses were found when using the Cl-EC:DEC formulation: a first cycle CE of as low as 50%.

When Cl-EC was used as an additive, the cycling performance was comparatively improved, with reasonable capacity retention although lower CE (performance statistics provided in Table S2 ESI†). However, it was observed that the capacity fade onset for the electrode tested with this Cl-EC used as an additive could vary significantly, commencing after as soon as *c.* 150 cycles or delayed until after *c*. 300 cycles.

When testing with EC:DEC, it was found that the long-term electrode performance would eventually result in erratic performance (sometimes as early as after several cycles, but typically after a few hundred cycles), which we attribute to the electroplating of lithium (we believe as a consequence of buildup of the EC-derived SEI which impedes ion transport into the electrode active material) that is followed by abrupt rises in cell resistance (selected snap-shots of the voltage profiles for this are shown in Fig. S8a ESI† along with other cycling tests showing erratic cycling behavior in Fig. S8b-c ESI†).[36]

By analysis of the differential capacity profiles of the electrode tested in EC:DEC through this 500 cycle test, it can be shown that the stable cycling observed prior to the *ca*. 270th cycle correlates with a consistently repeated voltage profile during charge (Fig. S9a-b ESI†). After the *ca*. 270th cycle, the capacity increases and this unusual behavior is accompanied by unstable capacities and coulombic efficiencies, recorded most obviously between cycles 300-450. By studying the voltage profiles (Fig. S9c-d ESI†), this added capacity is found to derive from charge accomplished at very low voltages, plausibly the result of localized lithium plating on the surface of the anode. This finding is consistent with the increasingly noisy differential capacity profiles in the low voltage domains after the *ca*. 270th cycle: rather than a consistently decreasing cell potential difference which is typical of even charging, the cell after the *ca*. 270th cycle appears to charge unsteadily, accomplishing a unit of charge with small, then large, then small changes in voltage. This behavior could be associated with localized lithium electroplating and dendrite growths arising from an increased tendency for ion accumulation on rather than transport through the higher impedance EC-derived SEI (further discussed in the section on AC impedance). For example, the drop observed in the voltage profile in the 400th cycle (Fig. S9c-d ESI†) is indicative of how wide-spread electroplating of lithium could lead to a cell in which the voltage abnormally quickly drops to a near-zero potential difference *vs* the lithium foil counter electrode.

Li-ion cycling at variable *C*-rates

Because the discharge voltage curve of cobalt oxide-based anodes results in (a) a high average discharge potential near 2 V and (b) voltage discharge over a continuum of potentials rather than at one or two voltage plateaus, we believe that the most likely application of a developed anode technology made from this material would likely not be for electric vehicles but for low-voltage portable electronics similar to the target market of Sony's *Nexelion* battery.[37]

The *Nexelion* anode uses a Sn/Co alloy particle which, like cobalt oxide anode materials, delivers its discharge continuously throughout a range of nearly 2 V rather than on one or multiple narrowly defined voltage plateaus like graphite, silicon or tin based anodes.[37] The higher capacity and longer cycle lifetime of the *Nexelion* anode as well as its performance at variable high *C*-rates are important advantages: besides addressing the need to provide greater capacity than the graphite type anode, alternative anode materials such as the Nexelion anode (that discharge through a range of potentials) might be attractive alternatives to graphite for use in low voltage electronics if these are able to charge at rapid rates.

In Fig. 3a-b, the capacity retention of the *meso*-porous Co_3O_4 electrode is shown at variable high rates up to 10*C*. The best performance was observed when using the 5% FEC in EC:DEC electrolyte: the electrode retained 100% of its conditioning cycle capacity after completing a 20 cycle series at 1*C* and 77% capacity retention after a series of 20 cycles at 5*C*. Eventually, after several cycles at 1*C* followed by a longer test of an additional 200 cycles at 5*C*, this capacity faded to 68% retention. After testing through 200 cycles at 10*C* rate and a third series of 200 cycles at 5*C*, the electrode performance stabilized with 60% retention. Then, upon returning to a 1*C* rate, the capacity recovered, recovering to a slightly higher (115% retention) capacity compared to the conditioning cycle capacity after a 100 cycle series (800 cycles total testing).

The results for using alternative electrolyte formulations for cobalt oxide-based anodes (statistics in Table S2a,b ESI†) can be evaluated in part by comparison to the results for the electrode cycled in the conventional EC:DEC which retained only 57% of its capacity after the first series (20 cycles) of testing at 5*C*. Typically, *C*-rate testing is conducted with intervals of 10 cycles at variable, progressively higher rates, concluding before 100 cycles of total testing. Here, the differences in electrode performance when tested with alternative electrolyte formulations become most notable only after the first hundred cycles. In the EC:DEC formulation, the electrode capacity exhibits significant fade when tested at a 5*C* rate for 200 cycles, from cycle numbers 120-319: at the end of this prolonged testing, the capacity retention is only 32% (vs the 68% retention for the electrode tested in the formulation employing FEC as additive). This retention may be attributed to the effect of the electrolyte, because we observed that after the testing reverted to a 1*C* rate after 720 cycles, the initial capacity was retained (106% retention), indicating that (a) that the electrode remained laminated to the current collector and (b) that the initial population of active material was still accessible for charge/discharge.

The comparative improvements made when using FEC:DEC, which retained 70% of its capacity after the 20 cycle 5*C* series and still 62% after the subsequent, extended 200 cycle series, were impressive gains compared to the results obtained when using EC:DEC. However, the actual capacity retention in FEC:DEC at high rates was consistently low when compared to the results when using FEC as an additive (*e.g.*, after the first 20 cycle initial 5*C* series, the capacity for the electrode in 5% FEC in EC:DEC was 631 mAh g^{-1} vs 490 mAh g^{-1} with FEC:DEC). The cycling results in terms of capacity retention and stability when using Cl-EC as an additive or co-solvent were comparatively poor, suggesting that this formulation results in a high-impedance ion transport barrier which restricts application to moderate rates of near 1*C* or lower for this electrode. When using Cl-EC as co-solvent, we believe that this high-impedance SEI is responsible for the unpredictable cell failures during long-term testing: after the impedance to ion transport increases beyond a certain limit, regions of the electrode may become inaccessible for future charging/discharging as the ions accumulate on or within the interphase rather than permeating through.

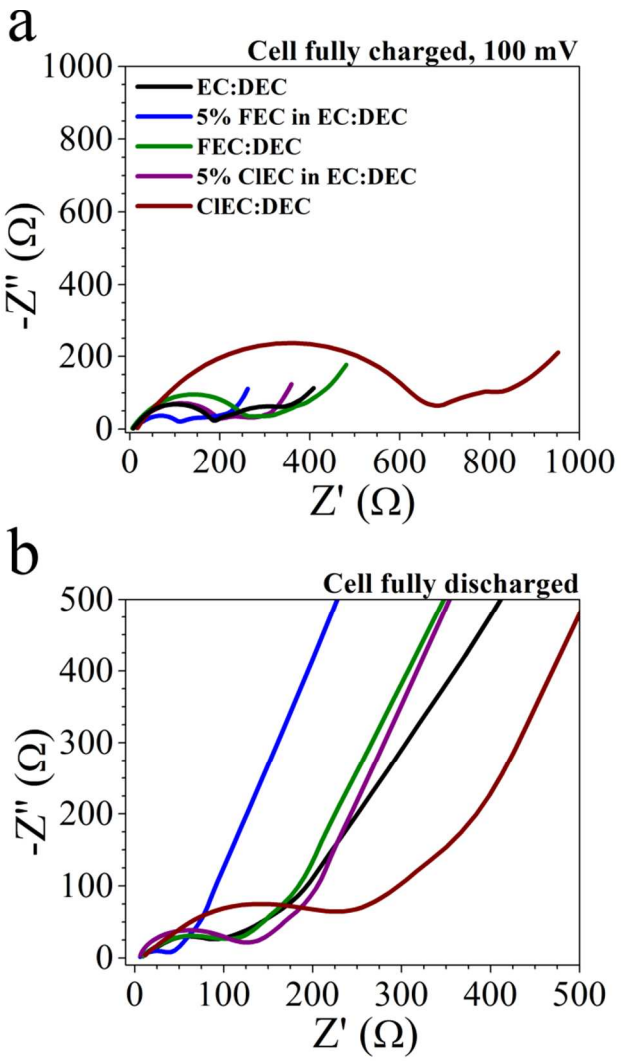

Fig. 5 AC impedance spectroscopy on *meso*-porous based Co_3O_4 electrodes at the fully charged and discharged state in the 10^{th} cycle of *C*/10 testing in half cells with EC:DEC, 5% FEC in EC:DEC, FEC:DEC, 5% Cl-EC in EC:DEC or Cl-EC:DEC electrolyte solvent formulations.

After these tests, the 5% FEC in EC:DEC electrolyte was selected for evaluation in a long-term, variable high *C*-rate test with an electrode made with higher active material composition (80% Co_3O_4 / 10% Super-P Li / 10% CMC) on an electrode of higher mass loading (1 mg cm^{-2}) in an effort to better assess the viability of the particle for use in a future anode. Similar to what was observed when using the lower content active material electrode (60% weight Co_3O_4), the high rate performance at 5*C* was relatively stable: after 200 cycles at 5*C*, the capacity retention was 525 mAh g^{-1}, 95% of the maximum 5*C* capacity and 59% of the theoretical 890 mAh/g (Fig. 4).

Through an additional 300 cycles at 5*C* (Fig. S10a ESI†), the capacity declined to 334 mAh g^{-1}, 60% of its 5*C* maximum value. After cycling stably with low capacity (~130 mAh/g) at 10*C*, the electrode tested at 5*C* for an additional 500 cycles and

its capacity declined slightly to 273 mAh g^{-1}, 50% of its 5*C* maximum. Then, upon returning to 1*C* rate, the electrode capacity recovered, cycling stably for 100 cycles to 962 mAh g^{-1}, 111% of its conditioning cycle capacity.

From this result, we attribute the gradual decline in capacity experienced during the 1,000 cycles of 5*C* testing to a rate limiting step during the ion transport. Despite this electrode being composed of 50% less conductive additive and binder, these cycling results – particularly the recovery of capacity after reverting to 1*C* rate after 1500 cycles – indicate the electrode performance did not suffer due to issues pertaining to electrode electrical conductivity or film delamination. Because of evidence indicating that these particles retained their morphology and because of the stable capacities observed during the first couple hundred cycles of this test, we believe that persistent irreversible reactions leading to an increasing thickness of SEI is responsible for the capacity decline observed. Indeed, the primary deficiency of the 5% FEC in EC:DEC formulation when compared to the next best alternative, FEC:DEC, is that the CE are lower, by an average of 0.5% during the 500 cycles of 1*C* testing.

In an effort to avoid increasing SEI growth and irreversible losses of Li ions, we experimented with a lower voltage cut-off potential, originally set at 10 mV. In the literature reporting on cobalt oxide-based anodes, the lower voltage cut-off potential is set at 5 or 10 mV in order to maximize charge capacity, particularly at high rates when kinetic limitations manifest. However, this choice of lower voltage cut-off does not reconcile with the selection of cobalt oxide as a safer alternative to graphite for an anode active material: besides its higher capacity, cobalt oxide, like other transition metal oxide materials, is a possible candidate for replacing the graphite electrode because it may allow for safer charging, without the hazard of electroplating and dendrite growth. The primary charging reactions (the reader is referred to detailed discussion of differential capacity profiles in ESI†) occur near 1.5 and 1.0 V (at 1*C* rate), which is far above the Li/Li^+ redox potential. In theory, a higher potential for the lower voltage cut-off when cycling cobalt oxide based anodes would allow for both complete charging of the active material (although perhaps not of the polymeric gel-like layer) and elimination of the hazard of electroplating and dendritic growths which contribute to irreversible losses and increasing SEI growth. This hypothesis was examined after the 1,500 variable high *C*-rate test when the cell returned to 1*C* rate testing. In (Fig. S10b ESI†) we observe that the average CE for this electrode cycled to 10 mV (cycles 1501-1600) at 1*C* was 98.35%, but when the lower voltage cut-off was raised to 100 mV, the average CE increased to 99.22% (cycles 1601-1650).

The decrease in side reactions was accompanied by diminished capacity, from an average of 932 mAh g^{-1} to 826 mAh g^{-1}. By adjusting the lower voltage cut-off potential, capacity decreased (by 106 mAh g^{-1}) but, significantly, irreversible losses were decreased by 60%, from 15.4 to 6.4 mAh g^{-1}. Adjustment of the lower voltage cut-off to 150 mV resulted in further attenuation of capacity to an average of 754 mAh g^{-1} and of irreversible losses to 4.2 mAh g^{-1} (corresponding to an average CE of 99.45%).

AC impedance spectroscopy

AC impedance spectroscopy was used to characterize the influence of the FEC or Cl-EC electrolyte formulations compared to a standard EC-based electrolyte on the impedance of Li-ion transport. The differences in cycling performance recorded when using the five electrolyte formulations can be analyzed in semi-quantitative terms by comparing their effect on the common steps of ion transport: bulk ion transport in the electrolyte, ion de-solvation (charge transfer), transport through the SEI and diffusion in the active material. The AC impedance spectra were collected at states of full charge (Fig. 5a) and discharge (Fig. 5b) after ten slow cycles at *C*/10 so that the effect of a fully developed SEI would be characterized, and the data was fitted to an equivalent circuit (Fig. S11a ESI†) commonly used to identify the impedance of these four transport steps in porous electrodes.[38]

The use of FEC or Cl-EC as additives or co-solvents was shown to have a significant effect on the activation energy required for de-solvation of the ion, the resistance to transport through the SEI and, surprisingly, also upon diffusion in the active material. The use of FEC or Cl-EC as electrolyte additives was expected to modify the SEI and the rate of ion transport through the interphase because these carbonates reduce more easily than EC: the energy of the lowest unoccupied molecular orbital (LUMO) for EC is 0.81 eV, compared to 0.37 eV for FEC and –0.43 eV for Cl-EC.[39] When FEC or Cl-EC was substituted for EC and used as a co-solvent, it was expected that there would also be a decrease in the resistance to charge transfer during de-solvation of the ion due to the lower binding energy of these carbonates to Li^+ in its solvation sheath.[39]

What we found from the AC impedance testing supported the results of our cycling tests, providing semi-quantitative analysis showing how the Li-ion transport is improved or impeded by the different electrolyte formulations. A comparison of the resistance to four transport steps for the electrode at full state of charge is shown in Fig. S11b ESI† (listed values provided in Table S4 ESI†).

The AC impedance spectra serve to indicate the physical basis for why the nominally identical electrodes perform so differently when cycled in alternative electrolytes. For the best capacity retention at high *C*-rate testing, FEC was used as an electrolyte additive. The use of this additive resulted in a modified SEI with only ~60% of the resistance to ion transport of the SEI derived from EC. This decrease in impedance through the SEI was accompanied by a decrease in the activation energy required for de-solvation of the ion. With this electrolyte formulation, the ion is exclusively solvated by EC[39,40] and so the decrease in resistance to this charge transfer step is attributed to the modified SEI stabilizing the de-solvation process.

While the use of FEC as a co-solvent resulted in a SEI with greater resistance (~50% more) to ion migration, this electrolyte

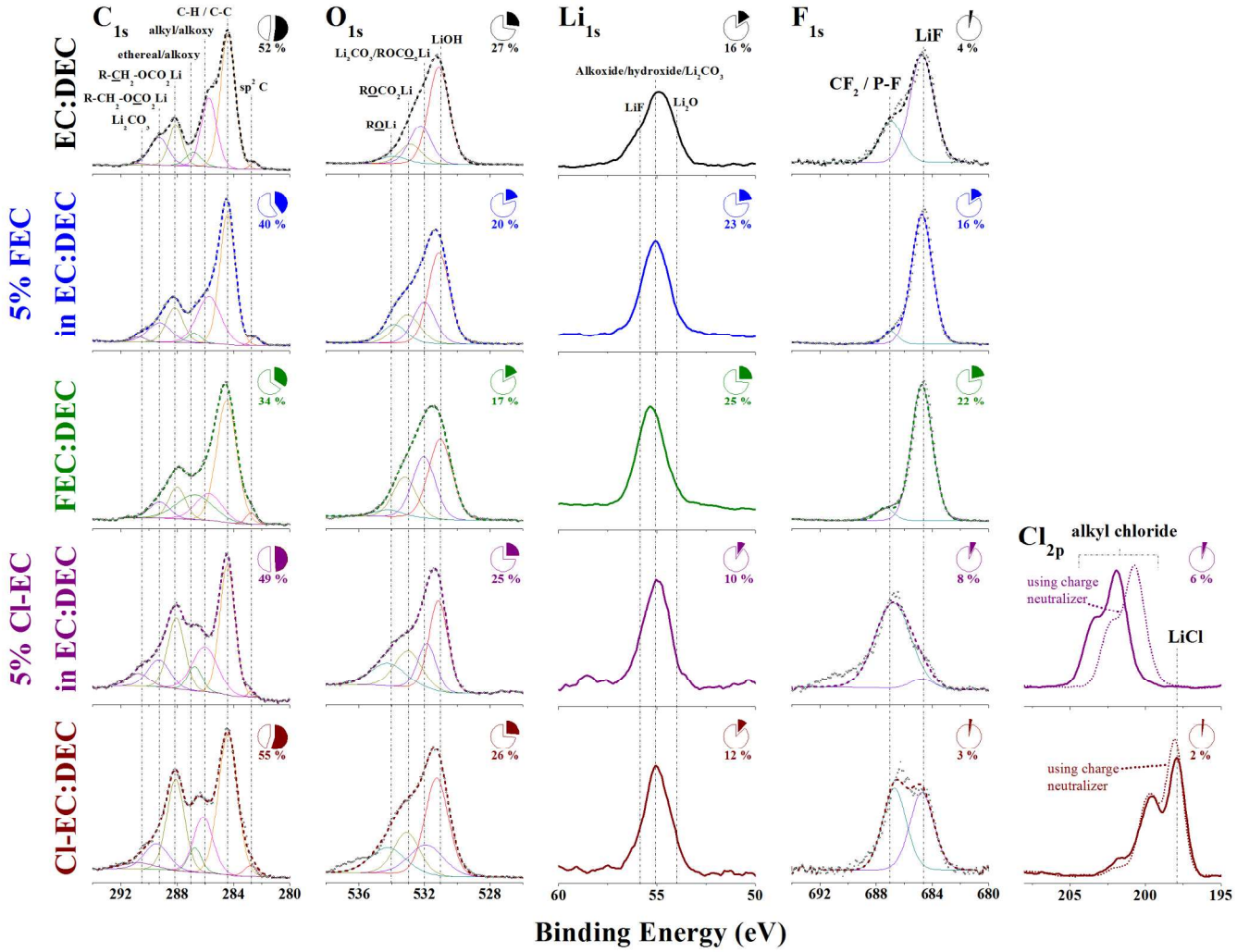

Fig. 6 XPS of SEI of the discharged anode after the 10th cycle of *C*/10 testing for each of the five electrolyte formulations evaluated. Species assignments are indicated by text and elemental composition is noted by the pie chart adjoining each regional spectra.

formulation resulted in further attenuation in the charge transfer resistance (greater than 90%), attributable to the interwoven effects of diminished Li^+/FEC bond energy in the solvation sheath and the surface chemistry of the SEI that facilitates de-solvation. The comparatively lower capacities (particularly at higher C-rates as recorded for electrodes tested in electrolytes with FEC as co-solvent rather than additive) are attributed to the higher resistance to ion transport through the SEI. The difference in transport rates might be ascribed to a combination of effects deriving from the chemistry and morphology of the SEI; the surface chemistry of these FEC-derived interphases (as well as those formed by Cl-EC containing electrolytes) was studied by XPS and these results are discussed further below.

The most stable cycling performance over 500 cycles testing at a rate of 1*C* was achieved using the FEC:DEC electrolyte but its use did not allow for as high of capacity retention at faster charge/discharge rates. This may be attributed to the comparatively greater resistance to ion migration through the exclusively-FEC derived SEI: 230% of the resistance for the 5% FEC in EC:DEC derived SEI. For the electrode cycled in Cl-EC:DEC, we observed far slower transport through the SEI and also in the particle bulk, as indicated by fitting the low-frequency data to a Warburg impedance element or, more specifically, the component of this element which describes diffusion length and diffusion rate (Fig. S11c ESI†). By using Cl-EC as an additive, the resistance to ion transport was comparable to what was found for the electrode cycled in EC:DEC and, as similar to what was observed when using FEC as an additive, the resistance to charge transfer was diminished. However, while the use of Cl-EC as an additive did increase the capacities recorded (particularly at higher rates) the cycling performance was not stable. Interestingly, good stability – 102% capacity retention *vs* the 10th cycle capacity – was observed for a meso-porous Co_3O_4 electrode tested with an electrolyte formulation of Cl-EC:FEC:DEC (1:1:2, volume %) through up to 1,000 cycles at 1*C* rate but with relatively poor, sub-99% CE (Fig. S12 ESI†).

XPS characterization of Li-ion SEI

XPS investigation of the SEI formed on the electrodes cycled 10 times at *C*/10 to their discharged state was conducted to complement the findings from AC impedance spectroscopy, which showed that resistance to ion transport (*via* migration through the SEI and de-solvation of the ion) is a function of SEI. Survey spectra and regional spectra (Fig. 6) were obtained to allow for a detailed analysis of the species present within the SEI. The method used to correct the spectra to account for charging and the references to the species assignments is found in the Experimental section. No signal was detected from the Co 2*p* region for any sample, indicating that the SEI thickness exceeded the *ca.* 10 nm thickness from which XPS signal is derived.

The SEI for the standard case – the SEI derived from the EC:DEC formulation – is dominated by C, O and Li signal (52, 27 and 16 atomic %, respectively), with only 4% F and less than 1 % P (these last elements derived from the reduction of the molten salt anion, PF_6^-). Several peaks can be deconvoluted from the C 1*s* and O 1*s* regional spectra, indicating this SEI is constituted of lithium hydroxide and of carbon species with mainly lower degrees of oxidation, principally sp^3 C-C and C-H and alkyl/alkoxide species (the percentage distribution of the C 1s spectra is provided in Fig. S13 ESI†) with a lesser amount of lithium alkyl-carbonate species. A portion of the alkyl/alkoxy signal is attributable to the carboxymethyl cellulose binder,[41] which is believed to be present within the bounds of the SEI interphase.

By including FEC as an additive, the chemistry of the SEI is significantly enriched by lithium fluoride. The F elemental composition is increased from 4 to 16 %, the overwhelming majority of which is found in lithium fluoride, a species which can be formed by the reactions of PF_5 and PF_6^- with Li, but in this instance is predominately generated by the decomposition of FEC. It has been reported that in the absence of EC, there is a more pronounced reduction of the PF_6^- ion[42] but for this electrolyte formulated with FEC only as an additive, this rationale does not apply. The correlation of increased concentration of LiF in the SEI and stable electrode cycling has been reported many times but the causation – how this species improves performance – remains restricted to informed speculation.[43]

Some reports link LiF to the formation of a thinner SEI which allows for more rapid ion transport as a consequence of its dimension.[22] Other reports suggest that a LiF-rich SEI is better able to withstand the volumetric changes which fracture an EC-derived SEI.[34] Based upon the results from AC impedance, we suggest another explanation: that with increasing LiF content, lithium ions are drawn more closely to and into the SEI, facilitating the ion desolvation process, as has been recently shown in a study employing atomistic modeling by Jorn et al.[44] Whether LiF is responsible for facilitating de-solvation as indicated by the experimental evidence, there appears to be a limit to its utility in improving overall ion transport; although the resistance to desolvation further diminishes with increase in content of LiF in the SEI found when using the FEC:DEC electrolyte formulation, the resistance to ion transport through the SEI increases markedly.

This resistance to transport is borne out in the cycling performance, particularly at higher *C*-rates, yet besides the already noted increase in LiF content, there is marginal difference in the regional spectra for the SEI derived from the electrolyte employing FEC as an additive or co-solvent. Measurements of the SEI morphology, the use of high-resolution XPS with careful depth profiling or evaluation of the SEI formed after cycling at higher rates may provide better insight into what distinguishes these SEI layers.

For the electrodes cycled in Cl-EC based formulations, there was a small uptake of Cl into the SEI (interestingly, more uptake for the formulation with Cl-EC as an additive) which differentiated its composition from that derived from EC:DEC or those using FEC. The most striking difference in the content of the Cl-EC derived SEIs was the relative amount of carbon, particularly lithium alkyl-carbonate and lithium carbonate species. From the fitting parameters imposed according to the results of prior works[29,42,45,46] focused on studying the reduction of electrolyte solvents and the composition of the SEI, we assigned the peaks representative of the content of the several carbon species. Notably, the lithium alkyl-carbonate and lithium carbonate species constituted about 25% of the SEI formed from the EC:DEC formulation but were over 35% for the Cl-EC formulations.

The rise in carbon-containing species came with an expected decrease in fluorine content but an unexpected decrease in lithium content, falling to near 10%. Taken with the AC impedance results, we believe that the higher content of carbonate species and lower content of lithium fluoride (or chloride) is responsible for the higher resistance of ion transport through the SEI, which was particularly evident for the Cl-EC:DEC formulation. It should be noted that the use of the charge neutralizer was employed for analysis of all regions due to the highly shifted chlorine signal for the SEI formed from 5% Cl-EC in EC:DEC. The dominant signal from the compensated spectra obtained using the charge neutralizer shows an oxidized chlorine containing species at near 200 eV which we were unable to confidently assign.

Evaluation of *meso*-Co_3O_4 for Na-ion batteries

The viability of *meso*-porous Co_3O_4 for use in a future Na-ion battery was examined with the same electrochemical tests and characterization performed for the Li-ion electrodes. These results complement and expand upon a recent communication reported by Rahman *et al.*,[47] indicating that Co_3O_4 is a potential candidate for use sodium ion battery anodes and also supporting their finding that the theoretical capacity of this active material is 447 mAh g^{-1} *vs* Na. By assuming a charge mechanism analogous to the conversion reaction with lithium, Klein *et al*. previously calculated that the sodium ion theoretical capacity remains 890 mAh g^{-1} with the free energy of formation of the Co + Na_2O (fully charged) phase formed at 0.84 V *vs* Na/Na^+.[48] However, in experiments, we find that even at low rates the reversible capacity of the electrode appears to be

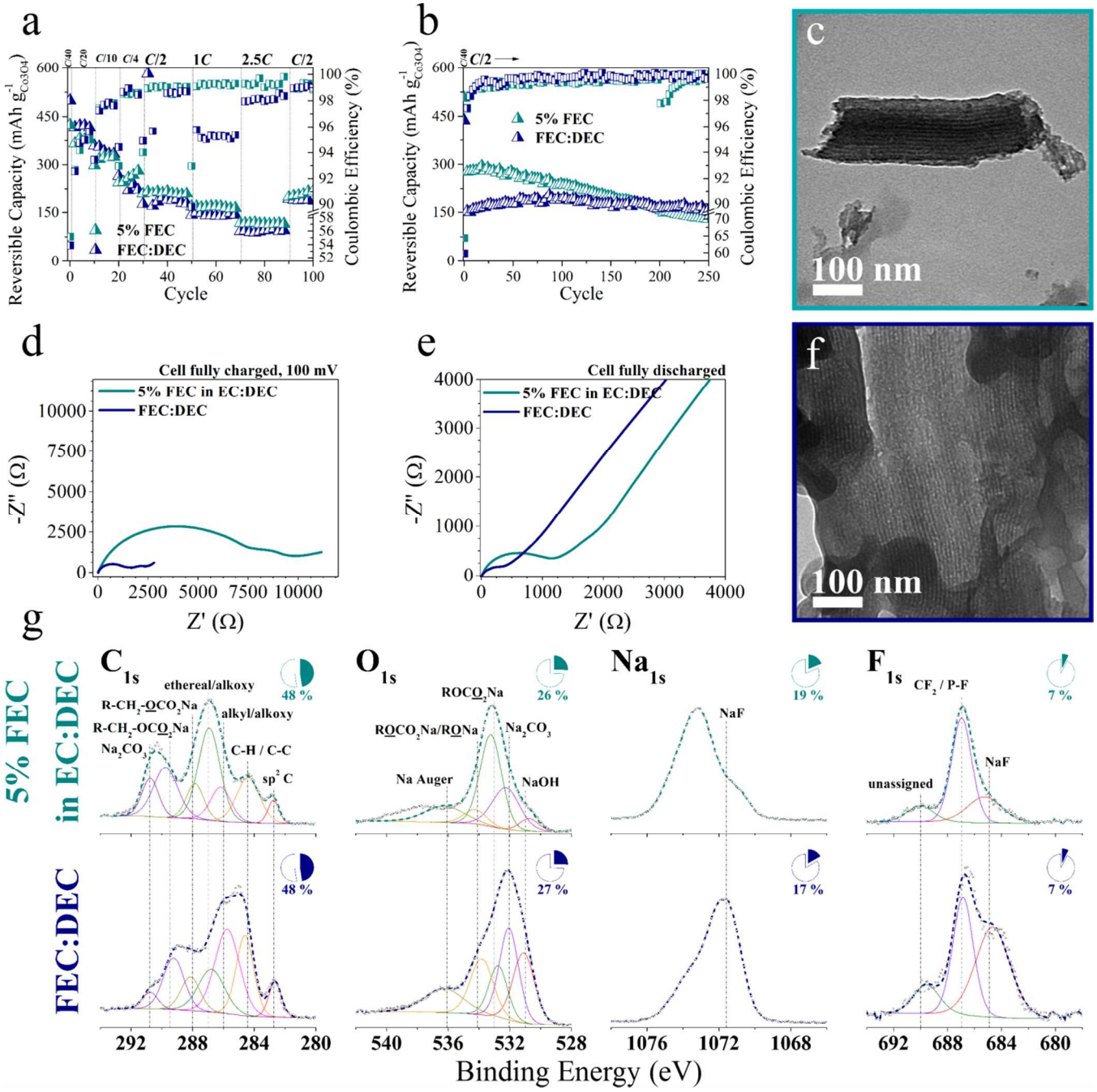

Fig. 7 Characterization of meso-porous Co_3O_4 when used as the active material for a Na-ion half cell, tested with two electrolyte formulations: 1M $NaPF_6$ in 5% FEC in EC:DEC and FEC:DEC. Electrochemical testing conducted (a) at variable *C*-rates and (b) to evaluate cycling stability at *C*/2 (0.445 mA/g) rate. AC impedance spectroscopy conducted at (a) fully charged and (b) discharged states in the 10th cycle of a *C*/20 test. After 250 cycles testing at *C*/2 rate, TEM done on ultramicrotomed sections of electrodes in discharged state showing meso-porous channels intact: (c) cycled in 5% FEC in EC:DEC and (f) cycled in FEC:DEC. XPS characterization of SEI formed in the discharged state for each electrode/electrolyte combination after the ten cycles testing at *C*/20 rate.

limited to only around half the theoretical value, near 445 mAh g^{-1}, in agreement with the finding of Rahman *et al*. This low capacity may be due to excessive cell internal resistance, for the differential capacity profile (Fig. S18 ESI†) indicates that the sodium charge/discharge reaction proceeds analogously to that of the lithium cell. Experiments are underway to verify the theoretical capacity by characterizing the mechanism of charge and discharge by means of *in-situ* Raman spectroscopy and *in-situ* XRD characterization. However, we believe that the mechanism proposed by Rahman *et al*. is more consistent with the cycling performance for the *meso*-porous particles tested here. Like Rahman *et al*., we find that at low *C*-rates the

electrode discharges reversibly to near 445 mAh g^{-1} but the more practically useful capacity at the relatively slow rate of 1*C* (0.89 A g^{-1}) was found to decrease to near 175 mAh g^{-1} using the best electrolyte formulations, 5% FEC in EC:DEC and FEC:DEC.

In this electrolyte survey, the EC:DEC formulation was omitted owing to its comparatively poor performance in several recent studies of Na-ion anode materials[49,50], while the majority of the coin cells tested with the Cl-EC:DEC and 5% Cl-EC in EC:DEC formulations were found to consistently fail after several cycles owing to internal shorting, likely a consequence of rapid sodium dendrite formation arising from poorly formed and/or high impedance SEIs, a problem which affected in lesser degree the Li-ion cells tested with analogous formulations.

In a variable rate test (Fig. 7a), the capacity retention for the electrode was similar using either of the FEC-type electrolyte formulations: at a rate of *C*/2 (455 mA g^{-1}), the retention was only 23% of the theoretical capacity (890 mAh g^{-1}) for the electrode in the 5% FEC formulation and 20% in the FEC:DEC formulation. However, in terms of stability (Fig. 7b), the electrode tested in FEC:DEC performed significantly better. At near 200 cycles, the electrodes provided near the same capacity, although the electrode tested in FEC:DEC retained 80% of its maximum 204 mAh g^{-1} capacity found during testing at *C*/2 (445 mA g^{-1}) through 200 cycles (and retained 75% capacity through 250 cycles) while the electrode cycled in 5% FEC retained only 53% through 200 cycles (44% through 250 cycles). The first cycle CE for the electrode tested in FEC:DEC was near 64%, slightly higher than the 60% value found for the 5% FEC formulation. The average CE during the first 200 cycles at *C*/2 (445 mA g^{-1}) was 99.7% when using FEC:DEC and a significantly lower 99.2% when using 5% FEC.

Irrespective of the electrolyte formulation used, the *meso*-porosity was retained as with the electrodes tested in lithium-ion cells; after 250 cycles at *C*/2, TEM was used to characterize ultramicrotomed sections of the electrodes in their full discharged state and the *meso*-porous channels were observed to be intact (Fig. 7c,f).

The differences in the cycling performance between the electrodes tested in the different electrolyte formulations as well as those differences in performance between electrodes tested with lithium *vs* sodium ions may be explained in part by the results of AC impedance spectroscopy taken after ten slow cycles at *C*/20 rate. Considering the electrode in its fully charged state (Fig. 7d), the impedance for the sodium ion electrodes is 1-2 orders of magnitude greater than that for lithium ion electrodes. The result of using FEC as a co-solvent rather than as an additive diminished the resistance to transport through the SEI by a factor of 6 and the charge transfer resistance by a factor of 2. (Tabulated values from fitted results found in Table S5 ESI†.)

As for the electrodes tested in lithium-ion cells, we attribute the differences in cycling performance – these derived in large measure from the ionic transport properties of the electrode system – to the chemistry and morphology of the SEI. The SEI formed on electrodes tested in sodium ion cells was characterized by XPS. In Fig. 7g, the regional spectra for the dominant elements is shown (the P signal is not shown as it accounted for about 1 atomic % in each SEI).

Compared to the SEI derived from lithium-ion salts, these SEI are constituted of a greater content of ether/alkoxy and carbonate species carbon species. As with the SEI derived from the Cl-EC:DEC formulation for the lithium-ion cell, the increased population of carbonates, alkyl-carbonates and ethers can be correlated to increased impedance to ion transport through the SEI and resistance to desolvation.

Following the parameters imposed according to the results of prior research into the Na-ion SEI,[51,52] the content of the various carbon species was found for these sodium-ion cell SEIs (Fig. S14 ESI†). The content of alkyl carbonates/carbonates for the SEI derived from the 5% FEC formulation was near 70% while only 43% for the SEI derived when FEC was employed as a co-solvent. While the presence of carbonate species appears to correlate with SEI in poorer performing cells, the increased content of NaF in the FEC:DEC derived SEI was observed to correlate with the more facile ion transport, this is possibly due to an analogous rationale to what has been suggested for the lithium-ion cell SEIs: the NaF species more strongly attracts the ion, facilitating its desolvation into the SEI.

Conclusions

The voltage characteristics of the cobalt oxide based anode recommend its consideration for use in low power portable electronics and other applications which might benefit from higher capacities and faster charge rates (at higher and therefore more safe voltages). We believe that the potential viability of a cobalt oxide-based anode is derived in part from progress in semiconductor technology that has led to the development of low voltage circuit architectures targeted toward extending battery life. For a recently developed model which optimizes via consideration of battery discharge and delay product, the desired V_{dd} was found to be 0.9 V for a simulation run for supply voltages ranging from 0.8-1.6 V for a VLSI circuit with 0.35u CMOS type transistors.[53]

Therefore, despite operating over a continuum of voltages, the low voltage requirements of modern semiconductors could allow for the possibility of a cobalt oxide based anode: when paired with a lithium cobalt oxide cathode, the average battery discharge potential at a C/10 rate is near 2.5 V: the average *meso*-porous cobalt oxide anode discharge potential at a C/10 rate vs Li/Li^+ is 1.68 V, and the average lithium cobalt oxide cathode charge potential at C/10 rate vs Li/Li^+ is near 4.2 V.[54]

With the stable structure of high surface area *meso*-porous Co_3O_4 particles in a conventional slurry cast electrode cycled using 1 M $LiPF_6$ in a mixture of 5 wt% FEC in (1:1 vol%) EC/DEC, we report good capacity retention at high rates: 77% retention at 5*C* and after testing through 800 cycles at variable *C*-rates, 115% capacity retention with stable cycling upon return to 1*C* rate. For highest capacity retention and coulombic efficiency over a calendar life test of 500 cycles at 1*C*, the co-

solvent mixture of (1:1 vol%) FEC:DEC is preferred: 92% capacity retention with an average CE of 99.6%.

The stable cycling even up to high rates that was observed in these tests may be attributed to a combination of factors: (a) the retention of the *meso*-porous structure that facilitates 1D ion transport down the *meso*-pores and appears to allow these particles to avoid the progressive segregation of Co into electrically isolated clusters as has been found previously and (b) the selection of alternative electrolyte formulations which form SEI with lower impedance to ion migration across the electrolyte/electrode interphase and which also facilitate ion desolvation, perhaps due to an increased content of ion-fluoride species which have been shown to have this effect in a recent atomistic modeling study.

The commonly used EC-based formulation (here a 1:1 vol% EC:DEC formulation is used) is not recommended due to worse cycling stability, retention at high *C*-rates, coulombic efficiency and, notably, safety concerns arising from a tendency for cells cycled with this electrolyte formulation to cycle irregularly (arising from abrupt cell resistance increases) after hundreds of cycles of testing.

In Na-ion testing, the potential for a *meso*-porous cobalt oxide based anode was demonstrated, with stable cycling performance and near 100% coulombic efficiencies observed at variable *C*-rates and during a 250 cycle test at 445 mA g^{-1} (*C*/2) rate. For best cycling stability, the electrolyte survey done here recommends the use of the 1M $NaPF_6$ in 1:1 (vol%) FEC:DEC formulation. Further, the experimental capacities reported here support the recent finding by Rahman *et al*. that an alternative mechanism exists for Co_3O_4 when charging/discharging *vs* Na, resulting in a theoretical capacity of 447 mAh g^{-1}.

Acknowledgements

The authors declare no competing interest. Financial support of this research was provided by the Robert A. Welch Foundation (CBM F-1436, AH F-1131, SMH F-1738) and acknowledgement is made to the Donors of the American Chemical Society Petroleum Research Fund for support of this research under grant 51948-DNI3 (S.G., S.M.H.). K.C.K. acknowledges the NSF Graduate Research Fellowship Program for financial support. K.C.K. thanks Dr. Hugo Celio, Dr. Karalee Jarvis and Dr. Elmer Klavetter.

Notes and references

Electronic Supplementary Information (ESI) available: [details of any supplementary information available should be included here]. See DOI: 10.1039/b000000x/

1. X.-J. Zhu, J. Hu, H.-L. Dai, L. Ding and L. Jiang, *Electrochimica Acta*, 2012, 64, 23-28.
2. X. Huang, H. Yu, J. Chen, Z. Lu, R. Yazami and H. H. Hng, *Advanced Materials*, 2014, DOI: 10.1002/adma.201304467, n/a-n/a.
3. J. Chen, X.-h. Xia, J.-p. Tu, Q.-q. Xiong, Y.-X. Yu, X.-l. Wang and C.-d. Gu, *Journal of Materials Chemistry*, 2012, 22, 15056-15061.
4. K. T. Nam, D.-W. Kim, P. J. Yoo, C.-Y. Chiang, N. Meethong, P. T. Hammond, Y.-M. Chiang and A. M. Belcher, *Science*, 2006, 312, 885-888.
5. Z. Hui, W. Jianbo, Z. Chuanxin, M. Xiangyang, D. Ning, T. Jiangping and Y. Deren, *Nanotechnology*, 2008, 19, 035711.
6. W. Mei, J. Huang, L. Zhu, Z. Ye, Y. Mai and J. Tu, *Journal of Materials Chemistry*, 2012, 22, 9315-9321.
7. L. Hu, N. Yan, Q. Chen, P. Zhang, H. Zhong, X. Zheng, Y. Li and X. Hu, *Chemistry – A European Journal*, 2012, 18, 8971-8977.
8. X. Wang, L. Yu, X.-L. Wu, F. Yuan, Y.-G. Guo, Y. Ma and J. Yao, *The Journal of Physical Chemistry C*, 2009, 113, 15553-15558.
9. N. Yan, L. Hu, Y. Li, Y. Wang, H. Zhong, X. Hu, X. Kong and Q. Chen, *The Journal of Physical Chemistry C*, 2012, 116, 7227-7235.
10. Y. Fu, X. Li, X. Sun, X. Wang, D. Liu and D. He, *Journal of Materials Chemistry*, 2012, 22, 17429-17431.
11. L. Li, G. Zhou, X.-Y. Shan, S. Pei, F. Li and H.-M. Cheng, *Journal of Power Sources*, 2014, 255, 52-58.
12. Y. Li, B. Tan and Y. Wu, *Nano Letters*, 2007, 8, 265-270.
13. Y. Xiao, C. Hu and M. Cao, *Journal of Power Sources*, 2014, 247, 49-56.
14. Y. Lu, Y. Wang, Y. Zou, Z. Jiao, B. Zhao, Y. He and M. Wu, *Electrochemistry Communications*, 2010, 12, 101-105.
15. X. Rui, H. Tan, D. Sim, W. Liu, C. Xu, H. H. Hng, R. Yazami, T. M. Lim and Q. Yan, *Journal of Power Sources*, 2013, 222, 97-102.
16. J. Sun, H. Liu, X. Chen, D. G. Evans and W. Yang, *Nanoscale*, 2013, 5, 7564-7571.
17. Z.-S. Wu, W. Ren, L. Wen, L. Gao, J. Zhao, Z. Chen, G. Zhou, F. Li and H.-M. Cheng, *ACS Nano*, 2010, 4, 3187-3194.
18. L. Zhan, Y. Wang, W. Qiao, L. Ling and S. Yang, *Electrochimica Acta*, 2012, 78, 440-445.
19. B. Zhang, Y. Zhang, Z. Miao, T. Wu, Z. Zhang and X. Yang, *J. Power Sources*, 2014, 248, 289-295.
20. K. M. Shaju, F. Jiao, A. Debart and P. G. Bruce, *Physical Chemistry Chemical Physics*, 2007, 9, 1837-1842.
21. N.-S. Choi, K. H. Yew, K. Y. Lee, M. Sung, H. Kim and S.-S. Kim, *Journal of Power Sources*, 2006, 161, 1254-1259.
22. H. Nakai, T. Kubota, A. Kita and A. Kawashima, *Journal of The Electrochemical Society*, 2011, 158, A798-A801.
23. A. M. Chockla, K. C. Klavetter, C. B. Mullins and B. A. Korgel, *ACS Applied Materials & Interfaces*, 2012, 4, 4658-4664.
24. Z. X. Shu, R. S. McMillan, J. J. Murray and I. J. Davidson, *Journal of The Electrochemical Society*, 1996, 143, 2230-2235.
25. N. Dahal, I. A. Ibarra and S. M. Humphrey, *Journal of Materials Chemistry*, 2012, 22, 12675-12681.
26. http://www.scribner.com/.
27. K. C. Klavetter, S. M. Wood, Y.-M. Lin, J. L. Snider, N. C. Davy, A. M. Chockla, D. K. Romanovicz, B. A. Korgel, J.-W. Lee, A. Heller and C. B. Mullins, *Journal of Power Sources*, 2013, 238, 123-136.
28. P. R. Abel, Y.-M. Lin, H. Celio, A. Heller and C. B. Mullins, *ACS Nano*, 2012, 6, 2506-2516.

29. S. Malmgren, K. Ciosek, M. Hahlin, T. Gustafsson, M. Gorgoi, H. Rensmo and K. Edström, *Electrochimica Acta*, 2013, 97, 23-32.
30. D. Larcher, G. Sudant, J.-B. Leriche, Y. Chabre and J.-M. Tarascon, *Journal of The Electrochemical Society*, 2002, 149, A234-A241.
31. Y.-M. Kang, M.-S. Song, J.-H. Kim, H.-S. Kim, M.-S. Park, J.-Y. Lee, H. K. Liu and S. X. Dou, *Electrochimica Acta*, 2005, 50, 3667-3673.
32. J. M. Zuo and J. C. Mabon, *Microsc Microanal*, 2004, 10.
33. K. Rhodes, M. Kirkham, R. Meisner, C. M. Parish, N. Dudney and C. Daniel, *Review of Scientific Instruments*, 2011, 82, 075107-075107-075107.
34. Y.-M. Lin, K. C. Klavetter, P. R. Abel, N. C. Davy, J. L. Snider, A. Heller and C. B. Mullins, *Chemical Communications*, 2012, 48, 7268-7270.
35. Y.-M. Lin, K. C. Klavetter, A. Heller and C. B. Mullins, *The Journal of Physical Chemistry Letters*, 2013, 4, 999-1004.
36. P. C. Howlett, D. R. MacFarlane and A. F. Hollenkamp, *J. Power Sources*, 2003, 114, 277-284.
37. D. Foster, J. Wolfenstine, J. Read and J. L. Allen, *Performance of Sony's Alloy Based Li-ion Battery*, S. a. E. D. Directorate Report ARL-TN-0319, Army Research Laboratory, Army Research Laboratory, 2008.
38. J. Liu and A. Manthiram, *Chemistry of Materials*, 2009, 21, 1695-1707.
39. M. H. Park, Y. S. Lee, H. Lee and Y.-K. Han, *J. Power Sources*, 2011, 196, 5109-5114.
40. K. Xu, Y. Lam, S. S. Zhang, T. R. Jow and T. B. Curtis, *The Journal of Physical Chemistry C*, 2007, 111, 7411-7421.
41. N. Pahimanolis, A. Salminen, P. Penttilä, J. Korhonen, L.-S. Johansson, J. Ruokolainen, R. Serimaa and J. Seppälä, *Cellulose*, 2013, 20, 1459-1468.
42. V. Etacheri, O. Haik, Y. Goffer, G. A. Roberts, I. C. Stefan, R. Fasching and D. Aurbach, *Langmuir*, 2011, 28, 965-976.
43. M.-J. Chun, H. Park, S. Park and N.-S. Choi, *RSC Advances*, 2013, 3, 21320-21325.
44. R. Jorn, R. Kumar, D. P. Abraham and G. A. Voth, *The Journal of Physical Chemistry C*, 2013, 117, 3747-3761.
45. A. M. Andersson and K. Edström, *Journal of The Electrochemical Society*, 2001, 148, A1100-A1109.
46. S. Chattopadhyay, A. L. Lipson, H. J. Karmel, J. D. Emery, T. T. Fister, P. A. Fenter, M. C. Hersam and M. J. Bedzyk, *Chemistry of Materials*, 2012, 24, 3038-3043.
47. M. M. Rahman, A. M. Glushenkov, T. Ramireddy and Y. Chen, *Chemical Communications*, 2014, 50, 5057-5060.
48. F. Klein, B. Jache, A. Bhide and P. Adelhelm, *Physical Chemistry Chemical Physics*, 2013, 15, 15876-15887.
49. P. R. Abel, Y.-M. Lin, T. de Souza, C.-Y. Chou, A. Gupta, J. B. Goodenough, G. S. Hwang, A. Heller and C. B. Mullins, *The Journal of Physical Chemistry C*, 2013, 117, 18885-18890.
50. D. Y. W. Yu, P. V. Prikhodchenko, C. W. Mason, S. K. Batabyal, J. Gun, S. Sladkevich, A. G. Medvedev and O. Lev, *Nat Commun*, 2013, 4, 2922.
51. S. Komaba, W. Murata, T. Ishikawa, N. Yabuuchi, T. Ozeki, T. Nakayama, A. Ogata, K. Gotoh and K. Fujiwara, *Advanced Functional Materials*, 2011, 21, 3859-3867.
52. S. Komaba, T. Ishikawa, N. Yabuuchi, W. Murata, A. Ito and Y. Ohsawa, *ACS Applied Materials & Interfaces*, 2011, 3, 4165-4168.
53. M. Pedram and Q. Wu, presented in part at the Proceedings of the 36th annual ACM/IEEE Design Automation Conference, New Orleans, Louisiana, USA, 1999.
54. *Lithium Batteries: Science and Technology*, Springer, 2003.